

Stability criterions of an oscillating tip-cantilever system in dynamic force microscopy

L.Nony^{*,1}, R.Boisgard², J.-P.Aimé²

¹ L2MP, UMR CNRS 6137, Université d'Aix-Marseille III

Faculté des Sciences de Saint-Jérôme, 13397 Marseille Cedex 20, FRANCE

² CPMOH, UMR CNRS 5798, Université Bordeaux I

351, cours de la Libération, 33405 Talence Cedex, FRANCE

* To whom correspondence should be addressed; E-mail: laurent.nony@l2mp.fr

PACS 05.45.-a, 07.79.Lh, 45.20.Jj

Submitted April 12, 2001, **published in European Physical Journal B 24, pp221-229 (2001)**

Abstract

This work is a theoretical investigation of the stability of the non-linear behavior of an oscillating tip-cantilever system used in dynamic force microscopy. Stability criterions are derived that may help to a better understanding of the instabilities that may appear in the dynamic modes, Tapping and NC-AFM, when the tip is close to a surface. A variational principle allows to get the temporal dependance of the equations of motion of the oscillator as a function of the non-linear coupling term. These equations are the basis for the analysis of the stability. One find that the branch associated to frequencies larger than the resonance is always stable whereas the branch associated to frequencies smaller than the resonance exhibits two stable domains and one unstable. This feature allows to re-interpret the instabilities appearing in Tapping mode and may help to understand the reason why the NC-AFM mode is stable.

I. INTRODUCTION

During the last decade, Dynamic Force Microscopy (DFM) used in the Tapping mode has been found as a suitable tool to investigate surface morphology, particularly of soft materials and has been widely used to investigate a very large range of samples including polymers^{1,2}, biological materials^{3,4} or organic layers^{5,6,7}. In recent years, the DFM was developed around the Non-Contact Atomic Force Microscopy (NC-AFM) mode and has shown that contrasts at the atomic scale could be achieved on semiconductors and insulators surfaces^{8,9,10,11,12,13}. Experimental and theoretical features dedicated to the description of these two dynamic modes have been widely discussed in previous papers^{14,15,16,17,18,19,20}. It was shown that the large sensitivity of the oscillating tip-cantilever system (OTCS) was based on the large value of its quality factor and on its non-linear dynamics in the vicinity of the surface^{21,22}. Even if the precise origin of the NC-AFM images contrast remains an open question, Tapping and NC-AFM results are the consequence of the same non-linear behavior of the OTCS so that their differences are purely technical. The aim of this article is to show from a theoretical point of view that the non-linear dynamics of the OTCS leads to various stability domains that may help to a better understanding of the way the instabilities appear in Tapping and the reason why the NC-AFM mode, while being so sensitive, keeps, in most of cases, a stable behavior.

The experimental study of the stability of the non-linear behavior of the OTCS can be performed through the study of approach-retract curves, from which are deduced the variations of the oscillations properties as a function of the tip-sample distance^{17,23}. But the ultimate goal of the approach-retract curves is to extract the surface properties from amplitude and phase variations (Tapping) or from frequency shift and damping signal (NC-AFM). In other words, the measure of the evolution of the amplitude with a fixed drive frequency and a drive amplitude or the one of the frequency shift are two complementary ways to investigate the non-linear behavior of the OTCS. Thus in this work, the analysis of the stability of the oscillations will be done from the study of the distortion of the resonance peak of the oscillator due to the coupling with the surface.

The paper is organized as follow. The first part is dedicated to a description of the non-linear behavior of the OTCS at the proximity of the surface. To do so, a specific

theoretical frame giving the explicit temporal dependance of equations of motion of the OTCS is developed. The description is then based on the equations of the stationary state of the OTCS that can be interpreted either for the Tapping or for the NC-AFM. In the second part, these equations are used to analyze the stability of the stationary state. The third part is a discussion of the results obtained and the way they can be interpreted for DFM experiments.

II. NON-LINEAR BEHAVIOR OF THE OTCS AT THE PROXIMITY OF A SURFACE

A. General features

The sketch of the OTCS and notations used in the present work are shown in fig.1. When a tip oscillates above a surface, several situations can occur. If the oscillation amplitude A is smaller than the distance D between the surface and the equilibrium position of the OTCS, the tip never touches the surface. On the contrary, for oscillation amplitudes larger than D , the tip exhibits intermittent contact situations. The time during which the tip touches the surface depends on several factors, among which, the local stiffness of the surface is a key parameter. For example, for very soft materials, the indentation depth can be as much as the oscillation amplitude²⁴, thus the tip spends half of the oscillation period into the substrate. For hard materials, the time during which the tip touches the surface is negligible compared to the oscillation period. Thus, when intermittent contact situations occur, various assumptions are required to describe the contact between the tip and the surface^{23,25,26}. For the present purpose, such an analysis introduces useless complications, therefore we only focus on the non-contact situations. When uniquely non-contact situations take place, the tip never touches the surface during the whole oscillation period so that the interaction between the tip and the surface can be described with a simple expression.

The attractive coupling force between the tip and the sample is assumed to derive from a sphere-plane interaction involving the disperse part of the Van der Waals potential²⁷. The differential equation describing the position of the tip's apex as a function of time, $z(t)$, is given by :

$$m^* \ddot{z}(t) + \frac{m^* \omega_0}{Q} \dot{z}(t) + k_c z(t) = \mathcal{F}_{exc} \cos(\omega t) - \nabla V_{int}[z(t)], \quad (1)$$

with :

$$V_{int}[z(t)] = -\frac{HR}{6[D - z(t)]} \quad (2)$$

ω_0 , Q , m^* and $k_c = m^* \omega_0^2$ are respectively the resonance pulsation, quality factor, effective mass and cantilever' stiffness of the OTCS. \mathcal{F}_{exc} and ω are the external drive force and drive pulsation. H , R and D are the Hamaker constant, the tip's apex radius and the distance

between the surface and the equilibrium position of the OTCS (see fig.1).

Different ways can be used to observe the non-linear behavior of the oscillating nanosphere at the vicinity of a surface. The most informative is to record several resonance curves as a function of the distance D ^{16,19,22,28}. Another possibility is to keep the oscillation at a given frequency with a fixed excitation amplitude and to record variations of the oscillation amplitude and of the phase as a function of D . This latter measurement is readily done by performing approach curves with the Tapping mode^{15,16,23,29}. As noted in the introduction, the difference between Tapping and NC-AFM is purely technical but, from a practical point of view, a description of the variation of the oscillating behavior showing the correspondence between the two modes is not straightforward. For example, the NC-AFM mode is probably the simplest way to describe a DFM experiment¹⁴, but the non-linear behavior appears in a quite subtle way while it is immediately observed with the Tapping mode.

The present section is divided into three parts. The first one details the specific theoretical frame for the obtention of the equations of motion in amplitude and phase of the OTCS. A coarse-grained method gives the equation describing the time evolution of the stationary state of the OTCS as a function of the coupling term between the tip and the surface. This allows to compute the stability of the stationary state. The next part is a description of the distortion of the resonance peak as a function of the distance. This provides the basis of the discussion about the oscillating behavior and the stability of the branches which is detailed in section III. This also provides an easier way to discuss experimental measurements as those obtained in Tapping and NC-AFM modes. As an example, we use the evolution of the resonance peak to discuss typical variations of the amplitude and phase in Tapping mode when the drive frequency is slightly below the resonance one²³. These variations, regularly observed, are the most obvious experimental evidences of the non-linear dynamics of the OTCS. The third part deals with the analysis of the resonance frequency shift observed in NC-AFM and the way its stability can be interpreted.

B. Theoretical frame

We search a solution to the temporal evolution of the OTCS by using a variational solution based on the principle of least action. Even though this approach exploits the same

physical concepts than the one which had led to the coupled equations in amplitude and phase of the stationary state of the OTCS^{17,22,23}, it appears to be more general since here, the temporal dependence is explicitly obtained. We start from the definition of the action of the OTCS coupled to an interaction potential :

$$S = \int_{t_a}^{t_b} \mathcal{L}(z, \dot{z}, t) dt, \quad (3)$$

where \mathcal{L} is the Lagrangian of the system²³ :

$$\begin{aligned} \mathcal{L}(z, \dot{z}, t) &= \mathcal{T} - \mathcal{V} + \mathcal{W} \\ &= \frac{1}{2}m^*\dot{z}(t)^2 - \left[\frac{1}{2}k_c z(t)^2 - z(t) \mathcal{F}_{exc} \cos(\omega t) + V_{int}[z(t)] \right] - \frac{m^*\omega_0}{Q} z(t)\dot{z}(t) \end{aligned} \quad (4)$$

Due to the large quality factor, we assume that a typical temporal solution is on the form :

$$z(t) = A(t) \cos[\omega t + \varphi(t)], \quad (5)$$

where $A(t)$ and $\varphi(t)$ are assumed to be slowly varying functions with time compared to the period $T = 2\pi/\omega$. The underlined variables of $\dot{z}(t)$:

$$\dot{z}(t) = \underline{\dot{A}}(t) \cos[\omega t + \underline{\varphi}(t)] - \underline{A}(t) [\omega + \underline{\dot{\varphi}}(t)] \sin[\omega t + \underline{\varphi}(t)],$$

are calculated along the physical path, thus they are not varied into the calculations³⁰. While among the trial functions solutions that can be chosen the present one is not the more general, the principle of least action ensures that functionals of this type are the best.

The equations of motion in amplitude and phase of the OTCS are obtained by considering the following coarse-grained operation. Let's assume a long duration $\Delta t = t_b - t_a$ with $\Delta t \gg T$ and calculate the action as a sum of small pieces of duration T :

$$S = \sum_n \int_{nT}^{(n+1)T} \mathcal{L}(z, \dot{z}, t) dt = \sum_n \left(\frac{1}{T} \int_{nT}^{(n+1)T} \mathcal{L}(z, \dot{z}, t) dt \right) T = \sum_n \mathcal{L}_e T \quad (6)$$

\mathcal{L}_e is the mean Lagrangian during one period and appears as an effective Lagrangian for a large time scale compared to the period. Owing to the quasi-stationary behavior of the amplitude and the phase over the period, the effective Lagrangian is calculated by keeping them constant during the integration. The calculations give :

$$\begin{aligned} \mathcal{L}_e(A, \dot{A}, \varphi, \dot{\varphi}) &= \frac{m^*}{4} [\dot{A}^2 + A^2(\omega + \dot{\varphi}^2)] - \frac{k_c A^2}{4} + \frac{\mathcal{F}_{exc} A \cos(\varphi)}{2} - \frac{1}{T} \int_0^T V_{int}[z(t)] dt \\ &\quad - \frac{m^*\omega_0}{2Q} [A \underline{\dot{A}} \cos(\varphi - \underline{\varphi}) - A \underline{A} (\omega + \underline{\dot{\varphi}}) \sin(\varphi - \underline{\varphi})] \end{aligned} \quad (7)$$

Note that the effective Lagrangian is now a function of the new generalized coordinates A , φ and their associated generalized velocities \dot{A} , $\dot{\varphi}$. At this point, remembering that the period is small regardless to $\Delta t = t_b - t_a$ during which the total action is evaluated, the continuous expression of the action is :

$$S = \int_{t_a}^{t_b} \mathcal{L}_e \left(A, \dot{A}, \varphi, \dot{\varphi} \right) d\tau, \quad (8)$$

where the measure $d\tau$ is such that $T \ll d\tau \ll \Delta t$.

Applying the principle of least action $\delta S = 0$ to the functional \mathcal{L}_e , we obtain the Euler-Lagrange equations for the effective Lagrangian :

$$\frac{d}{d\tau} \left(\frac{\partial \mathcal{L}_e}{\partial \dot{A}} \right) - \frac{\partial \mathcal{L}_e}{\partial A} = 0 \quad \text{and} \quad \frac{d}{d\tau} \left(\frac{\partial \mathcal{L}_e}{\partial \dot{\varphi}} \right) - \frac{\partial \mathcal{L}_e}{\partial \varphi} = 0 \quad (9)$$

The amplitude and phase equations of motion of the OTCS coupled to an interaction potential $V_{int}[z(t)]$ are :

$$\begin{cases} \ddot{A} = \left[\left(\frac{\omega}{\omega_0} + \dot{\varphi} \right)^2 - 1 \right] A - \frac{1}{Q} \dot{A} + \frac{\mathcal{F}_{exc} \cos(\varphi)}{k_c} - \frac{\omega}{\pi k_c} \frac{\partial I(A, \varphi)}{\partial A} \\ \ddot{\varphi} = - \left(\frac{2\dot{A}}{A} + \frac{1}{Q} \right) \left(\frac{\omega}{\omega_0} + \dot{\varphi} \right) - \frac{\mathcal{F}_{exc} \sin(\varphi)}{k_c} \frac{1}{A} - \frac{\omega}{\pi k_c} \frac{1}{A^2} \frac{\partial I(A, \varphi)}{\partial \varphi} \end{cases}, \quad (10)$$

with :

$$I(A, \varphi) = \int_0^T V_{int}[z(t)] dt \quad (11)$$

The system given by eqs.10 is defined for any kind of interaction potential and no particular hypothesis are required to perform the calculations. This implies that, provided that $I(A, \varphi)$ is analytical, the equations of motion can be obtained for any kind of non-linearity. For instance, in ref.³¹, analogous calculations were performed for the Duffing's oscillator. If we consider the sphere-plane interaction involving the disperse part of the Van der Waals potential (see equ.2), it was shown²³ that :

$$I(A, \varphi) = - \frac{\pi H R}{3\omega} \frac{1}{\sqrt{D^2 - A^2}} \quad (12)$$

Thus :

$$\frac{\partial I(A, \varphi)}{\partial A} = - \frac{\pi H R}{3\omega} \frac{A}{(D^2 - A^2)^{3/2}} \quad \text{and} \quad \frac{\partial I(A, \varphi)}{\partial \varphi} = 0 \quad (13)$$

Using usual dimensionless notations²³, the equs.10 of the coupled equations of motion becomes :

$$\begin{cases} \ddot{a} = [(u + \dot{\varphi})^2 - 1] a - \frac{\dot{a}}{Q} + \frac{\cos(\varphi)}{Q} + \frac{a\kappa_a}{3(d^2 - a^2)^{3/2}} \\ \ddot{\varphi} = -\left(\frac{2\dot{a}}{a} + \frac{1}{Q}\right)(u + \dot{\varphi}) - \frac{\sin(\varphi)}{aQ} \end{cases}, \quad (14)$$

$d = D/A_0$ is the reduced distance between the location of the surface and the equilibrium position of the OTCS normalized to the resonance amplitude $A_0 = Q\mathcal{F}_{exc}/k_c$, $a = A/A_0$ is the reduced amplitude, $u = \omega/\omega_0$ is the reduced drive frequency normalized to the resonance frequency of the free OTCS and $\kappa_a = HR/(k_c A_0^3)$ is the dimensionless parameter that characterizes the strength of the interaction. The explicit dependance of the coupling term κ_a with the oscillation amplitude through the power law A_0^{-3} indicates the non-linear character of the dynamics.

C. Resonance peak and amplitude variation recorded during a Tapping experiment

The equations of motion of the stationary solutions a and φ are obtained by setting $\dot{a} = \dot{\varphi} = 0$ and $\ddot{a} = \ddot{\varphi} = 0$ in equ.14 and lead to two coupled equations of the sine and cosine of the phase of the OTCS previously calculated²³ :

$$\begin{cases} \cos(\varphi) = Qa(1 - u^2) - \frac{aQ\kappa_a}{3(d^2 - a^2)^{3/2}} \\ \sin(\varphi) = -ua \end{cases}, \quad (15)$$

Solving equ.15 gives the relationship between the sweep frequency and the amplitude at a given distance d^{22} :

$$u_{\pm}(a) = \sqrt{\frac{1}{a^2} - \frac{1}{4Q^2} \left(1 \mp \sqrt{1 - 4Q^2 \left(1 - \frac{1}{a^2} - \frac{\kappa_a}{3(d^2 - a^2)^{3/2}} \right)} \right)^2} \quad (16)$$

The signs plus and minus are deduced from the sign of $\cos(\varphi)$ and correspond to values of the phase ranging from 0 to -90° (u_- , $\cos(\varphi) > 0$) or from -90° to -180° (u_+ , $\cos(\varphi) < 0$), in agreement with the sign convention of the phase in equ.5. From equ.16 is calculated the resonance peak at any reduced distance for a given strength of the sphere-surface interaction.

The two branches define the distortion of the resonance peak as a function of d . u_- gives the evolution of the resonance peak for frequency values below the resonance one and u_+ for frequency values above the resonance.

For the description of a Tapping experiment, the variation of the amplitude a as a function of the distance d is readily obtained by rewriting equ.16 as follow :

$$d_{\pm} = \sqrt{a^2 + \left[\frac{Q\kappa_a}{3 \left\{ Q(1-u^2) \mp \sqrt{1/a^2 - u^2} \right\}} \right]^{2/3}} \quad (17)$$

Consequently, depending on the drive frequency and the drive amplitude (through the A_0^{-3} dependance into κ_a), bifurcations from a stable to a bistable state may occur leading to amplitude and phase jumps. From an experimental point of view, the conditions required for the appearance of the bifurcations have been extensively discussed in refs.^{17,23}. In particular, the use of drive frequencies lower than the resonance frequency favor the measurement of the bifurcations corresponding to the non-contact situations.

In figs.2 and 3 are given the distortion of the resonance peak and the evolution of the amplitude as a function of d for an identical set of parameters. For large values of d , e.g. when the surface is far from the OTCS (point K), the non-linear effects are negligible and the peak keeps a well-defined Lorentzian shape (see equ.16 with $\kappa_a = 0$). When the OTCS is approached towards the surface, because the interaction is attractive, the resonance peak starts to distort towards the low frequencies. The distortion of the peak increases as d decreases. In the vicinity of the resonance, $u \lesssim 1$, $a \gtrsim 1$ and for small values of d the branches u_+ and u_- become very close. To mimic a Tapping experiment, the drive frequency is fixed to u_{drive} in fig.3. With the parameters used, at $d_1 = 2$ the oscillations properties are nearly identical to those at d infinite. When the peak starts to distort the amplitude and the phase (not shown) vary (L). In the present example, because u_{drive} is chosen below the resonance, the amplitude first increases. When the OTCS is further approached it reaches an unstable branch (M) and jumps to the stable branch (N) such that the bistable structure of the oscillator can be experimentally observed. At a closer distance, the peak further distorts and the amplitude is reduced since it follows the variations of u_+ (point O on fig.3). Then, when the oscillator is retracted, it follows the upper stable branch until the resonance value corresponds to the fixed frequency u_{drive} (point P on fig.3) and then jumps down to the lower stable branch. The curve exhibits a hysteresis cycle (points M, N, P and L). On

the figs.2 and 3, the branches that are supposed unstable are shown with dashed lines.

D. Resonance frequency shift

Using equ.16, the resonance frequency shift as a function of the distance d is obtained by setting $a = 1$. This former condition ensures the required condition for the NC-AFM mode. Thus, the normalized frequency shift, $(\nu - \nu_0) / \nu_0$, is given by $u - 1$ ²² :

$$u_{\pm}(d) - 1 = \sqrt{1 - \frac{1}{4Q^2} \left(1 \mp \sqrt{1 + \frac{4}{3} \frac{Q^2 \kappa_a}{(d^2 - 1)^{3/2}}} \right)^2} - 1 \quad (18)$$

In fig.4 is given the frequency shift as a function of the distance d for the same set of parameters than the one of figs.2 and 3. Following the previous discussion about the stability of the different parts of the resonance peak during the distortion, since the measure is performed as a function of d with $a = 1$, no bistable behavior can be observed. The OTCS follows the same branch u_- or u_+ whose location is always stable whatever the peak distortion.

Nevertheless, note that it should exist only one branch of variation for the frequency shift which is defined from the condition $a = 1$. But two branches are obtained as a consequence of the two solutions d_{\pm} . When the peak is distorted, the branches u_- and u_+ become very close as Q becomes large (see for instance, fig.2 with $d_3 = 1.012$). Therefore even with an oscillation amplitude kept constant, question rises about the ability of the OTCS to remain on the same branch. Qualitatively, one may expect that around $a \cong 1$, the branch u_- is unstable and u_+ is stable (see fig.2). If this is true, any small fluctuation of the oscillation amplitude might produce a jump from one branch to the other one as discussed in ref.²². Since the branch u_- seems to be unstable, a jump to this branch should lead to an abrupt decrease of the amplitude, which in turn might produce an apparent abrupt decrease of the quality factor. Because such a jump should show accidents, both on the resonance frequency shift curve and on the damping signal, accidents which are, in most cases, not observed, it becomes useful to determine more accurately the stability of the two branches.

The main aim of the variational method is to define a theoretical frame describing at the same time the evolution of all the variables : a , φ , u and d of the OTCS dynamics. Thus, it becomes useless to discuss about the stability of each kind of branch for the two dynamic

modes since the stability of a given couple (a, φ) , or (a, u) as a function of d can be deduced for any other couple. The discussion will be made on the branches of the resonance peak.

III. STABILITY CRITERIONS

The stability of the branches u_{\pm} of the resonance peak (see equ.16) is obtained from equations of motion of the OTCS (see equ.14). These equations are linearized around the stationary solution which will be now identified by the index “s”. At this stage, we fall into the well-known linear theory (see for instance refs.³² and³³). Writing into a four dimensions matrix the linearized system corresponding to the generalized coordinates (a, φ) and their associated generalized velocities $(\dot{a}, \dot{\varphi})$, we extract the eigenvalues and discuss the stability as a function of the sign, negative (stable solution) or positive (unstable solution), of their real part. The calculations are detailed in the appendix.

The stability criterion for each one of the two branches is given by the following inequation (see equ.29) :

$$\left(\frac{u}{Q}\right)^2 - (u^2 - 1 + \Delta) \frac{\cos(\varphi_s)}{Qa_s} > 0 \quad (19)$$

Δ is proportional to κ_a (see appendix, equ.22), thus characterizes the non-linear attractive coupling term. Solving the associated equality gives the critical branch u_{\pm}^{crit} whose location regardless u_{\pm} defines the stability of each branch. Unfortunately, u_{\pm}^{crit} has no simple expression. Therefore the stability condition 19 can not be exploited as is. Nevertheless a numerical routine allows to get its main features. The fig.5(a) shows the distortion of the resonance peak and the critical branch u_{\pm}^{crit} numerically computed for each branch. u_{+}^{crit} never crosses u_{+} and is always located below it. On the contrary, u_{-}^{crit} crosses u_{-} twice and their relative position depends on the value of the amplitude which, in turn, is going to define two domains of stability. The figs.5(b) and 5(c) are zooms on the regions α and β of u_{-} . The intersection spots are exactly located where the curvature of u_{-} changes. Therefore it's worth discussing the stability as a function of the local curvature of the branches u_{\pm} and so introducing their derivative da_s/du_{\pm} . As shown in the appendix, the inequation 19

can be summarized as follow :

$$\left\{ \begin{array}{l} \frac{da_s}{du} > 0 \quad \text{and} \quad \cos(\varphi_s) > a_s/(2Q) \quad (i) \\ \text{or} \\ \frac{da_s}{du} < 0 \quad \text{and} \quad \cos(\varphi_s) < a_s/(2Q) \quad (ii) \end{array} \right. \quad (20)$$

The aim of this former expression is to exhibit an explicit and particularly simple dependence of the stability of the branches as a function of their derivative :

↔ For the u_+ branch, da_s/du_+ being always negative and the associated value of the phase being always defined beyond -90° (see section II C), thus $\cos(\varphi_s) < 0$, the criterion (ii) implies that the u_+ branch is always stable, whatever the value of a_s .

↔ Concerning u_- , the sign of the derivative changes twice. For this branch, the phase is always defined above -90° which in turn means $\cos(\varphi_s) > 0$. Therefore on the lower part of the branch (small a), $da_s/du_- > 0$ and the criterion (i) indicates that the branch is locally stable. When da_s/du_- becomes negative (see fig.5(b)), because $\cos(\varphi_s)$ is still positive, the criterion (i) is no more filled. As a consequence, u_- is locally unstable and the instability is precisely located where the infinite tangent appears. On the upper part of the resonance peak, the curvature of u_- changes again and $da_s/du_- > 0$ (see fig.5(c)), implying that it is again a locally stable domain. Thus the branch u_- exhibits two stable domains and one unstable.

Note also that the resonance condition is deduced from $da_s/du = 0$ which implies $\cos(\varphi_s) = a_s/(2Q)$. This equality is the usual resonance condition of a free harmonic oscillator. If $a_s = 1$, e.g. without any coupling, the resonance phase is therefore $\varphi_s = \arccos[1/(2Q)]$. For the OTCS we used, $Q \simeq 500$, and so $\varphi_s \simeq -90^\circ$.

IV. DISCUSSION

The previous criterions allow to conclude to the stability of the OTCS for each dynamic mode. It was shown that, for an attractive coupling, the branch u_+ was always stable and that the instability was controlled by u_- . For frequencies lower than the resonance (branch u_-), when the tangent da_s/du_- is positive, the branch is stable. Thus, there is a small domain close to the resonance value for which the u_- branch remains stable.

For the Tapping, this result implies that the OTCS is locked on a stable branch until $da_s/du_- \rightarrow \pm\infty$ (see figs.2 and 3, point M) which makes the amplitude jumping up to the upper stable branch u_+ (point N on fig.3) during the approach and jumping down to the lower stable one u_- (point P) during the retract.

For the NC-AFM, the result of the present work shows that u_+ is always stable but that also a small domain of u_- around the resonance value remains stable. If the resonance value would have been located at the point where da_s/du_- is infinite, an infinitely small fluctuation would have been able to generate a catastrophic behavior like large variations of the oscillation amplitude and lead to an abrupt increase of the damping signal as previously discussed and suggested in ref.²².

Nevertheless, the size of the u_- stable domain is Q dependant. The more the Q factor is large, the more the size of the domain is reduced. The fig.6 illustrates the reduction of the size of the domain for $Q = 500$ and $Q = 5000$. With $Q = 5000$, the size of the domain is so weak that it nearly no appears on the scale of the figure. As a consequence, even if the previous discussion may help to understand why abrupt increases of the damping signal do not systematically occur, question remains unclear for the very high Q factors that can be obtained in ultra-high vacuum ($Q \gtrsim 10000$). At this step, it's worth giving orders of magnitude. During a NC-AFM experiment, an electronic feedback loop keeps constant the amplitude of the OTCS and locks its phase at -90° . Therefore question rises about the size of the stable domain in phase around -90° . If any fluctuation around the locked value goes beyond the stable domain, the OTCS behavior becomes unstable. For $Q = 500$, the size of the stable domain is of about 1.5° whereas it's reduced to 0.15° for $Q = 5000$ (data not shown). Thus, if the electronic loop is able to control the phase locking with a better accuracy than 0.15° , the OTCS will be locked within a stable domain and in turn won't give rise to instabilities. In addition, since the ability of the electronic loop to control the oscillating behavior depends on the value of the quality factor³⁴, the reduction of the domain of stability might not be a key parameter.

Practically, during our experiments, even with quality factors larger than 10000, drastic variations of the oscillation amplitude are never observed. Thus, the main aim of the present work is to show that, if the oscillator is properly locked at the -90° value throughout an experiment, this value corresponds to a stable domain.

V. CONCLUSION

This paper was a theoretical investigation of the stability of the non-linear behavior of an oscillating tip-cantilever system close to a surface. A variational principle has allowed to get the temporal dependance of equations of motion of the oscillator as a function of the non-linear attractive coupling. The interaction potential chosen is a disperse Van der Waals one, calculated between a sphere and a plane. The stationary state is obtained and can be interpreted either in the Tapping mode or in the NC-AFM mode. The stability of the stationary state is analyzed in terms of distortion of the resonance peak as a function of the coupling. It is found that stability criterions can be expressed from a simple inequality involving the sign of the derivative of the curve. The branch associated to the frequencies larger than the resonance is always stable whereas the branch associated to the frequencies smaller than the resonance exhibits two stable domains. The instability appears when the branch exhibits an infinite tangent. This feature allows to re-interpret the instabilities appearing in Tapping mode and may help to understand why the NC-AFM mode is stable most of time.

Appendix: Computation of the stability of the branches

Let's note $a = a_s(1 + \xi)$ and $\varphi = \varphi_s + p$ with $\xi, p \ll 1$. The index s is attributed to the stationary solution. Keeping the terms of first order in equ.14, equations of motion of the variations ξ and p regardless a_s and φ_s respectively, may be written as :

$$\begin{cases} \ddot{\xi} = (u^2 - 1 + \Delta)\xi + \frac{u}{Q}p - \frac{1}{Q}\dot{\xi} + 2u\dot{p} \\ \ddot{p} = -\frac{u}{Q}\xi - \frac{\cos(\varphi_s)}{Qa_s}p - 2u\dot{\xi} - \frac{1}{Q}\dot{p} \end{cases}, \quad (21)$$

with :

$$\Delta = \frac{\kappa_a}{3(d^2 - a_s^2)^{3/2}} \left(1 + \frac{3a_s}{d^2 - a_s^2} \right) \quad (22)$$

The system is solved by setting $\Xi = \dot{\xi}$, and $\Psi = \dot{p}$ leading to a linear system of the fourth order :

$$\begin{pmatrix} \dot{\xi} \\ \dot{p} \\ \dot{\Xi} \\ \dot{\Psi} \end{pmatrix} = \mathbb{M} \begin{pmatrix} \xi \\ p \\ \Xi \\ \Psi \end{pmatrix}, \quad (23)$$

with :

$$\mathbb{M} = \begin{pmatrix} 0 & 0 & 1 & 0 \\ 0 & 0 & 0 & 1 \\ u^2 - 1 + \Delta & u/Q & -1/Q & 2u \\ -u/Q & -\cos(\varphi_s)/(Qa_s) & -2u & -1/Q \end{pmatrix} \quad (24)$$

The eigenvalues of the matrix are obtained by solving the characteristic polynom given by $P = \det(\mathbb{M} - \lambda\mathbb{I})$. P can then be written as :

$$P = (\lambda^2 + \lambda/Q + M) (\lambda^2 + \lambda/Q + N) \quad (25)$$

By identification :

$$\begin{cases} M + N = 3u^2 + 1 - \Delta + \frac{\cos(\varphi_s)}{Qa_s} \\ MN = (u/Q)^2 - (u^2 - 1 + \Delta) \frac{\cos(\varphi_s)}{Qa_s} \end{cases} \quad (26)$$

The characteristic equation $P = 0$ is then equivalent to the following system :

$$\begin{cases} \lambda^2 + \lambda/Q + M = 0 \\ \lambda^2 + \lambda/Q + N = 0 \end{cases} \Leftrightarrow \begin{cases} \lambda_{1,2} = \left(-1/Q \pm \sqrt{(1/Q)^2 - 4M} \right) / 2 \\ \lambda_{3,4} = \left(-1/Q \pm \sqrt{(1/Q)^2 - 4N} \right) / 2 \end{cases} \quad (27)$$

The stable solutions are the ones given by $\Re(\lambda_i) < 0$ ³², thus :

$$\begin{cases} 1/Q > \sqrt{(1/Q)^2 - 4M} \\ \text{and} \\ 1/Q > \sqrt{(1/Q)^2 - 4N} \end{cases} \Leftrightarrow M > 0 \quad \text{and} \quad N > 0 \quad (28)$$

According to relationships 26, two conditions are necessary to fill equ.28 and in turn to ensure the stability of the solutions : $MN > 0$ and $M + N > 0$.

↪Let's first consider $MN > 0$ which is the main of the both (see below) :

$$MN = \left(\frac{u}{Q}\right)^2 - (u^2 - 1 + \Delta) \frac{\cos(\varphi_s)}{Qa_s} > 0 \quad (29)$$

The equation $MN = 0$ can be numerically solved using a Maple routine. Nevertheless a tractable stability criterion requires to write in a different way the expression 29. Using the relationship $\cos(\varphi_s) = \pm\sqrt{1 - (ua_s)^2}$ (see equ.15), the two coupled equations of the sine and cosine of the phase of the stationary state imply :

$$G(a_s, u) = Qa_s(1 - u^2) - g(a_s) \mp \sqrt{1 - (ua_s)^2} = 0, \quad (30)$$

with :

$$g(a_s) = \frac{a_s Q \kappa_a}{3(d^2 - a_s^2)^{3/2}} \quad (31)$$

Therefore :

$$dG(a_s, u) = \partial_{a_s} G(a_s, u) da_s + \partial_u G(a_s, u) du = 0, \quad (32)$$

and so :

$$\frac{da_s}{du} = -\frac{\partial_u G(a_s, u)}{\partial_{a_s} G(a_s, u)} \quad (33)$$

The calculations lead to :

$$\frac{da_s}{du} = \frac{u}{Q} \times \frac{2 \cos(\varphi_s) - a_s/Q}{\left(\frac{u}{Q}\right)^2 - (u^2 - 1 + \Delta) \frac{\cos(\varphi_s)}{Qa_s}} \quad (34)$$

The denominator is exactly the product MN , thus :

$$MN > 0 \Leftrightarrow \frac{u}{Q} \times \frac{2 \cos(\varphi_s) - a_s/Q}{\frac{da_s}{du}} > 0 \quad (35)$$

u/Q being always positive, the stability condition $MN > 0$ is reduced to :

$$\frac{2 \cos(\varphi_s) - a_s/Q}{\frac{da_s}{du}} > 0 \Leftrightarrow \begin{cases} \frac{da_s}{du} > 0 & \text{and} & \cos(\varphi_s) > a_s/(2Q) \\ & \text{or} & \\ \frac{da_s}{du} < 0 & \text{and} & \cos(\varphi_s) < a_s/(2Q) \end{cases} \quad (36)$$

↪ Let's now consider the condition $M + N > 0$:

$$M + N = 3u^2 + 1 - \Delta + \frac{\cos(\varphi_s)}{Qa_s} > 0 \quad (37)$$

Considering that a_s varies within the range $[0.1 + \varepsilon]$, with $1 \gg \varepsilon > 0$, it's straightforward to show that the inequality is always filled so that the stability criterions are only given by the condition $MN > 0$ and equ.36.

References

-
- ¹ Stocker, W., Beckmann, J., Stadler, R., Rabe, J.P. Surface reconstruction of the lamellar morphology in a symmetric poly(styrene-block-butadiene-block-methyl methacrylate) triblock copolymer: A tapping mode scanning force microscope study. *Macromolecules*, 29(23):7502–7507, 1996.
 - ² Magonov, S.N., Elings, V., Denley, D. , Wangbo, M.H. Tapping-mode atomic force microscopy study of the near-surface composition of a styrene-butadiene-styrene triblock copolymer film. *Surf. Sci.*, 389:201–211, 1997.
 - ³ Rivetti, C., Guthold, M., Bustamante, C. Scanning force microscopy of DNA deposited onto mica: Equilibration versus kinetic trapping studied by statistical polymer chain analysis. *J. Mol. Biol.*, 264:919–932, 1996.
 - ⁴ Shlyakhtenko, L.S., Gall, A.A., Weimer, J.J., Hawn, D.D., Lyubchenko, Y.L. Atomic force microscopy imaging of DNA covalently immobilized on a functionalized mica substrate. *Biophys. J.*, 77:568–576, 1999.
 - ⁵ Schwartz, D.K., Steinberg, S., Israelachvili, J., Zasadzinski, J.A.N. Growth of a self-assembled monolayer by fractal aggregation. *Phys. Rev. Lett.*, 69(23):3354–3357, 1992.

- ⁶ Barrat, A., Silberzan, P., Bourdieu, L., Chatenay, D. How are the wetting properties of silanated surfaces affected by their structure? an atomic force microscopy study. *Europhys. Lett.*, 20(7):633–638, 1992.
- ⁷ Vallant, T., Brunner, H., Mayer, U., Hoffmann, H., Leitner, T., Resch, R., Friedbacher, G. Formation of self-assembled octadecylsiloxane monolayers on mica and silicon surfaces studied by atomic force microscopy and infrared spectroscopy. *J. Phys. Chem. B*, 102:7190–7197, 1998.
- ⁸ Geissibl, F.J. Atomic resolution of the silicon (111) – 7×7 surface by atomic force microscopy. *Science*, 267:68–71, 1995.
- ⁹ Sugarawa, Y., Otha, M., Ueyama, H., Morita, S. Defect motion on an *InP*(110) surface observed with noncontact AFM. *Science*, 270:1646–1648, 1995.
- ¹⁰ Kitamura, S., Iwatsuki, M. Observation of the silicon surfaces using UHV non-contact AFM. *Jpn. J. Appl. Phys.*, 35:L668–L671, 1996.
- ¹¹ Bammerlin, M., Lüthi, R., Meyer, E., Baratoff, A., Lü, J., Guggisberg, M., Gerber, C., Howald, L., Güntherodt, H.J. True atomic resolution on the surface of an insulator via ultrahigh vacuum dynamic force microscopy. *Probe Microscopy*, 1:3–9, 1996.
- ¹² Schwarz, A., Allers, W., Schwarz, U.D., Wiesendanger, R. Simultaneous imaging of the in and as sublattice on *inas* (110) – (1×1) with dynamic scanning force microscopy. *Appl. Surf. Sci.*, 140:293–297, 1999.
- ¹³ Bennowitz, R., Bammerlin, M., Guggisberg, M., Loppacher, C., Baratoff, A., Meyer, E., Güntherodt, H.-J. Aspects of Dynamic Force Microscopy on NaCl/Cu(111): Resolution, Tip-Sample Interactions and Cantilever Oscillation Characteristics. *Surf. Interface Anal.*, 27:462, 1999.
- ¹⁴ Albrecht, T.R., Grütter, P., Horne, D., Rugar, D. Frequency modulation detection using high-q cantilevers for enhanced force microscope sensitivity. *J. Appl. Phys.*, 69(2):668–673, 1991.
- ¹⁵ Anczykowski, B., Krüger, D., Fuchs, H. Cantilever dynamics in quasiconnact force microscopy: Spectroscopic aspects. *Phys. Rev. B*, 53(23):15485–15488, 1996.
- ¹⁶ Wang, L. Analytical descriptions of the tapping-mode atomic force microscopy response. *Appl. Phys. Lett.*, 73(25):3781–3783, 1998.
- ¹⁷ Boisgard, R., Michel, D., Aimé, J.-P. Hysteresis generated by attractive interaction: Oscillating behavior of a vibrating tip-microlever system near a surface. *Surf. Sci.*, 401:199–205, 1998.
- ¹⁸ *Proceedings of the First International Workshop on Noncontact Atomic Force Microscopy*. Appl.

- Surf. Sci., Osaka (Japan) July 21-23, 1998.
- ¹⁹ Sasaki, N., Tsukada, M. Theory for the effect of the tip-surface interaction potential on atomic resolution in forced vibration. *App. Surf. Sci.*, 140(3-4):339–343, 1999.
- ²⁰ *Proceedings of the Second International Workshop on Noncontact Atomic Force Microscopy*. Appl. Surf. Sci., Pontresina (Switzerland), September 1-4, 1999.
- ²¹ Aimé, J.-P., Couturier, G., Boisgard, R., Nony, L. Relationship between the non linear behaviour of an oscillating tip-microlever system and the contrast at the atomic scale. *Appl. Surf. Sci.*, 140:333–338, 1999.
- ²² Aimé, J.-P., Boisgard, R., Nony, L., Couturier, G. Nonlinear dynamic behaviour of an oscillating tip-microlever system and the contrast at the atomic scale. *Phys. Rev. Lett.*, 82(17):3388–3391, 1999.
- ²³ Nony, L., Boisgard, R., Aimé, J.-P. Nonlinear dynamical properties of an oscillating tip-cantilever system in the tapping mode. *J. Chem. Phys.*, 111(4):1615–1627, 1999.
- ²⁴ Marsaudon, S., Leclère, Ph., Dubourg, F., Lazzaroni, R., Aimé, J.-P. Quantitative measurement of the mechanical contribution to tapping-mode atomic force microscopy. images of soft materials. *Langmuir*, 16:8432–8437, 2000.
- ²⁵ Garcia, R., San Paulo, A. Attractive and repulsive tip-sample interaction regimes in tapping-mode atomic force microscopy. *Phys. Rev. B*, 60(7):4961–4967, 1999.
- ²⁶ Dubourg, F., Aimé, J.-P. Role of the adhesion between a nanotip and a soft material in the tapping mode. *Surf. Sci.*, 466:137–143, 2000.
- ²⁷ Israelachvili, J.N. *Intermolecular and Surface Forces*. Academic Press, New York, 2nd edition, 1992.
- ²⁸ Gleyzes, P., Kuo, P.K., Boccara, A.C. Bistable behavior of a vibrating tip near a solid surface. *Appl. Phys. Lett.*, 58(25):2989–2991, 1991.
- ²⁹ Bachelot, R., Gleyzes, P., Boccara, A. Influence of both repulsive and attractive force fields in tapping mode atomic force microscopy. *Probe Microscopy*, 1:89–97, 1997.
- ³⁰ Goldstein, H. *Classical Mechanics*. Addison-Wesley, Reading, 1980.
- ³¹ Nony, Laurent. *Analysis of the Dynamic Force Microscopy : Application to the Study of DNA*. PhD thesis, University Bordeaux I, 4th of December, 2000.
- ³² Manneville, P. *Structures Dissipatives, Chaos et Turbulences*. Aléa Saclay, 1991.
- ³³ Gutzwiller, M.C. *Chaos in Classical and Quantum Mechanics*. Springer-Verlag, 1991.

³⁴ Couturier, G., Aimé, J.-P., Salardenne, J., Boisgard, R. A virtual non-contact atomic force microscope (NC-AFM) : Simulation and comparison with analytical models. to be published in European Physical Journal Applied Physics, 2001.

Figures

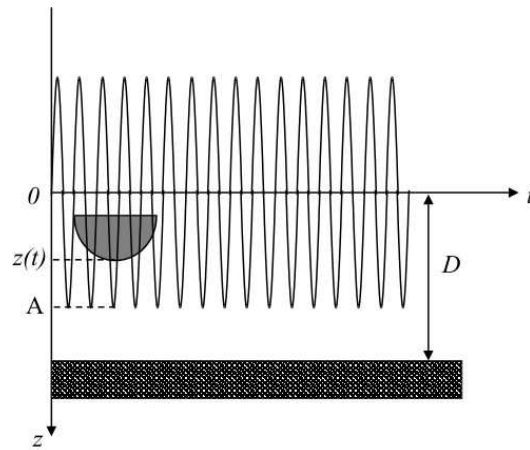


FIG. 1: Sketch of the OTCS and notations used.

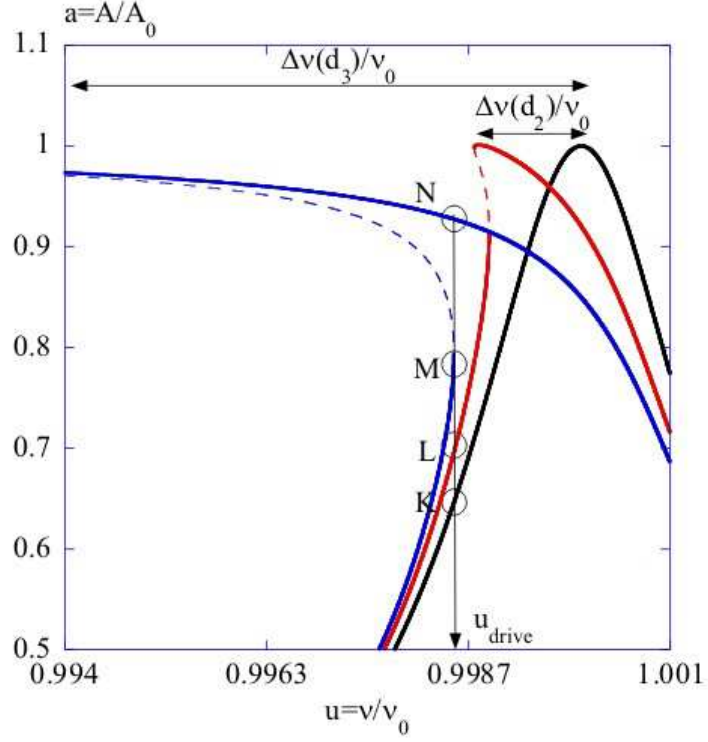


FIG. 2: Evolution of the resonance peak computed from equation (16) for three values of the distance, $d_1 = 2$, $d_2 = 1.11$ and $d_3 = 1.012$. The numerical parameters are $A_0 = 20$ nm, $Q = 400$ and $\kappa_a = 8 \times 10^{-4}$. For an attractive coupling, the peak is more and more distorted towards the low frequencies as d is reduced, e.g. the surface is approached and lead to the bifurcations observed on the tapping curve (Fig. 3, point M) when the drive frequency, $u_{drive} = 0.9985$, is chosen below the resonance and to the variations of the resonance frequency shift (Fig. 4). For each value of d , the unstable domains of u_- are shown with dashed lines.

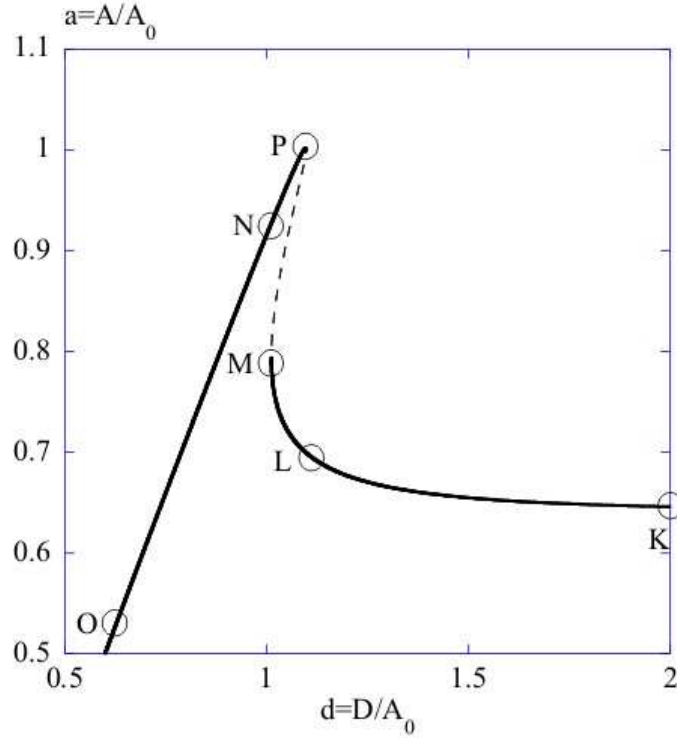


FIG. 3: Variations of the amplitude as a function of the distance, e.g. approach-retract curve in the tapping mode computed from equation (17). The numerical parameters are the same than in Figure 1 and the drive frequency chosen is $u_{drive} = 0.9985$. The curve exhibits a hysteresis cycle (MNPL) due to the non-linear coupling that characterizes bifurcations (points M and P) from a monostable to a bistable state (see text). The stable domains of the branches are shown with continuous lines and the unstable domain with dashed line.

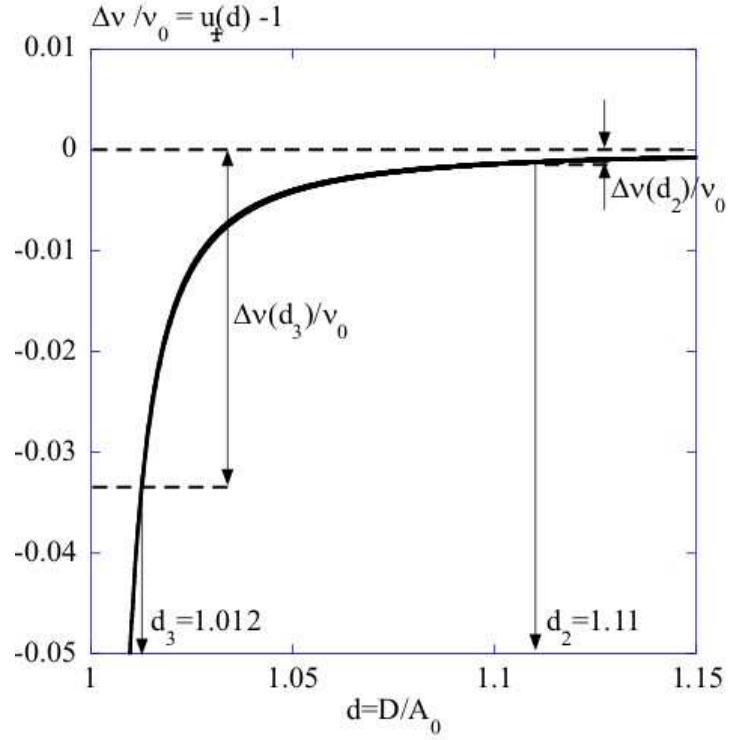


FIG. 4: Variations of the frequency shift of the resonance peak of the oscillator as a function of the distance, e.g. approach-retract curve in NC-AFM mode computed from equation (18). The numerical parameters are the same than in Figure 1. It's predicted that the curve is stable with d .

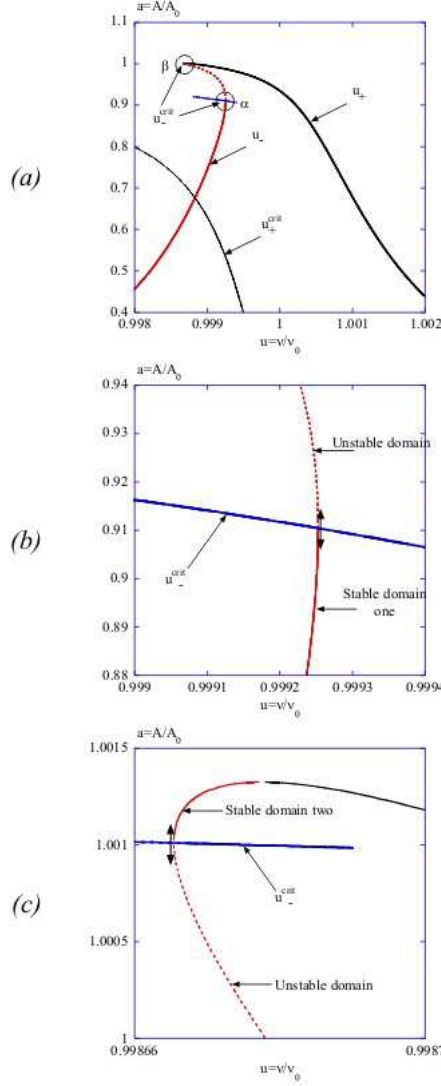


FIG. 5: (a) Distortion of the resonance peak computed from equation (16). The numerical parameters are $d = 1.05$, $A_0 = 10$ nm, $Q = 500$ and $\kappa_a = 2.5 \times 10^{-4}$. The critical branches u_{\pm}^{crit} are calculated from equation (19). u_+ is always located above its critical branch u_+^{crit} and in turn is always stable. u_-^{crit} crosses u_- twice. This leads to define three domains to describe the stability of the branch. The domains are defined between the spots where the derivative da/du_- diverges (see text). (b) Zoom in the region α of u_- . The stability criterion foresees that below u_-^{crit} , u_- is stable and unstable above. This is illustrated by the dashed lines. (c) Zoom in the region β of u_- . As da/du_- diverges again, it defines a new domain of u_- which is predicted to be stable.

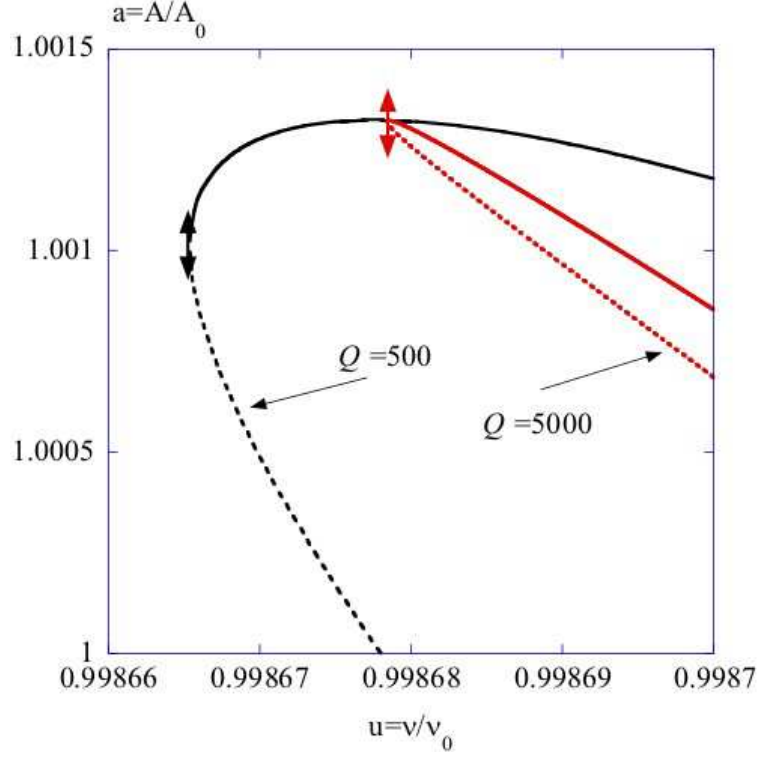


FIG. 6: Zoom on the same scale than Figure 5c of the distortion of the resonance peak for two values of the quality factor of the OTCS, $Q = 500$ and $Q = 5000$. The numerical parameters are the same than in Figures 5. The unstable domain of u_- is still shown with dashed lines but the size of the second stable domain is drastically reduced for the larger value of Q so that it nearly no appears on this scale. The associated phase variations regardless -90° (not shown) are of about 1.5° and 0.15° for $Q = 500$ and 5000 , respectively (see text).